TÜBİTAK

Turkish Journal of Earth Sciences

http://journals.tubitak.gov.tr/earth/

Research Article

Turkish J Earth Sci
(2023) 32: 915-930

doi:10.55730/1300-0985.1882

A study on the magnetite skarn mineralization (Gümüşhane, Türkiye): a magnetic survey

Ferkan SİPAHİ[1,*], M. Burhan SADIKLAR[2], Mehmet Ali GÜCER[1], Ali AYDIN[3], Rasim Taylan KARA[4]

[1]Department of Geological Engineering, Gümüşhane University, Gümüşhane, Turkiye
[2]Department of Geological Engineering, Karadeniz Technical University, Trabzon, Turkiye
[3]Department of Geological Engineering, Pamukkale University, Denizli, Turkiye
[4]Graduate Education Institute, Gümüşhane University, Gümüşhane, Turkiye

Received: 12.05.2023 • **Accepted/Published Online:** 07.10.2023 • **Final Version:** 17.11.2023

Abstract: Iron (Fe)-skarn mineralizations (Çambaşı, Dereli, Eğrikar, Karadağ, Kopuz, Sekü, Donguldere, Arnastal, Özdil, Ögene, İkizdere, Ovit Dağı, Kartiba, etc.) in the eastern part of the Pontides (NE Türkiye) are accommodated in the Pontide paleomagmatic arc and the eastern part of the Pontides Metallogenic Belt containing numerous various deposits. Fe-skarn mineralization around the Arnastal Plateau (Gümüşhane-Türkiye) is fragmentary in this area, which is covered with plants (grasses, flowers, etc.). Thus, it was attempted to describe the subsurface structures and Fe mineralization using an interpretation of the available geological and existing magnetic data in this area. Granitoid and volcano-sedimentary series (Upper Cretaceous) outcrop in the study area. These volcano-sedimentary series consist of limestone, sandy limestone, marl, andesite, quartz andesite, basalt, and their equivalent pyroclastics. They include a thin layer of the red limestone (Upper Cretaceous) and olistolith recrystallized limestones (Jurassic-Lower Cretaceous). Zigana granitoid, intruding into all of these rocks, is high-K calc-alkaline and metaluminous and is classified as quartz monzonite, monzogranite, granite, and syenogranite as a result of its modal composition. Contact pyrometasomatic mineralization occurs in between the limestone and granitoids in the Arnastal Plateau. In addition to petrographic and mineralogical studies, magnetic methods were applied to an area of approximately 10 km^2 to find any covered Fe deposits. Magnetic susceptibility values measured on the outcropped rocks ranged from 1 to 34 (10^{-7} SI) for limestone, 78 to 3750 (10^{-7} SI) for basalt, and 105 to 3946 (10^{-7} SI) for granitoids. It is considered that these ranges express the alteration (physical or chemical) of the rocks, their homogeneity, and the lack or presence of Fe minerals. The magnetic survey was conducted along a study area measuring 12,075 m long with 25 and/or 50 m station spacing. Processing of the magnetic data revealed the presence of eight buried Fe ores that could represent either massive or disseminated mineralization between the Sarıtaş and Kurtdere plateaus. Magnetite ore bodies may be present from the surface to a depth of approximately 15–25 m inside the limestone. In addition to the identification of new magnetite ore mineralization or bodies, a new geological map was designed by determining probable formation boundaries with this magnetic survey.

Key words: Granitoid, magnetite skarn, magnetic method, susceptibility, Türkiye

1. Introduction

Many methods have been developed to determine the location and depth of sources that cause magnetic anomalies (Bilim and Ateş, 2003). Mineral exploration in locations where mineralization is linked to altered rocks is useful due to the successful application of rock magnetic techniques (Haidarian Shahri et al., 2010; Pandarinath et al., 2023). Magnetic prospecting is one of the most effective methods used to determine geological structures containing iron (Fe) ore. Fe is one of the most common elements in the Earth's crust, and is constructed of magnetite minerals in addition to some heavy elements (Au, Ag, Cu, Mn, Cr, Fe-titanium, some Fe-sulfide) and oxygen (Mekkawi, 2012). Magnetite deposits containing ferrous minerals, which extend from the Earth's surface to a depth of 1500 m, can be determined effectively via magnetic techniques (Ergin, 1985). The source of magnetic susceptibility in rocks is magnetite, titanomagnetite, ilmenite, pyrrhotite, and ferromagnesian silicate minerals. Additionally, border analysis and normalized full-grade methods are used to determine the position of a buried object with magnetic features (Elmas and Babacan, 2021). In previous studies (e.g., Ishihara, 1977; Ishihara et al., 2000), the magnetic susceptibility of granitic rocks was successfully used to distinguish between magnetite- and ilmenite-series granites using a crude petrographic index. Magnetic susceptibility is also considered as a reliable method in exploration studies (Pandarinath et al. 2014, 2019). Magnetic susceptibil-

* Correspondence: ferkansipahi@gmail.com

ity of granitoids is highly changeable and has the potential to uncover petrographic and geochemical variations (e.g., Aydın, 1994; Sipahi, 1996; Aydın et al., 1997, 2007; Ishihara et al., 2000; Vincent et al., 2013; Villaseca et al., 2017). In recent years, studies on paleomagnetism in the Pontides, especially in the Cretaceous and Eocene periods, have increased (Aydın et al., 2007; Çinku et al., 2009, Meijers et al., 2010; Çinku et al., 2010a, 2010b, 2011, 2015; Cengiz, 2023). Aydın et al. (2007) showed that magnetic susceptibility studies in the Saruhan Granitoids (NE Türkiye) had an important potential for petrologic exploration in magnetite-series granitic rock. Çinku et al. (2009) investigated the rock magnetic and geochemical characteristics of Upper Cretaceous volcanic rocks in the Pontides (N–NE Türkiye) and determined that the magnetic properties could be interpreted in terms of the concentration, composition, and magma generation. Magnetic data is used as an indicator of spatial distribution, volume, and concentration of magnetically significant minerals (Büyüksaraç et al., 2005; Adagunodo et al., 2015; Navaanchimed et al., 2015).

Thus, this study examined whether there is a mineralization at any depth and aimed to determine the geometry and extent of the magnetite skarn mineralization underneath the surface at the Arnastal Plateau in the eastern Black Sea region (NE Türkiye). The choice of the study area was motivated by the fact that it represents a former mine site, which hosts fragmented deposits. The area is covered by grass, and the use of magnetic prospecting can aid in detecting new buried magnetite ores.

2. Geological setting

The NE Black Sea region of Türkiye hosts the Alpin Metallogenic Belt, which includes skarn mineralization, one of the different types of ore mineralizations in the belt (Figure 1a). The eastern Black Sea Metallogenic Belt, which developed from the Jurassic to the Miocene during the subduction of the Tethyan oceanic crust, is regarded as a magmatic arc (Dixon and Pereira, 1974). The epoch from the Late Triassic to Early Jurassic is regarded as the birth of the Neotethys Ocean during the closure of the Paleotethys Ocean (Şengör and Yılmaz, 1981; Dokuz and Sünnetçi, 2019). The Late Jurassic-Early Cretaceous is characterized by platform-type carbonates and less magmatic rocks. The Late Cretaceous rocks in the eastern Sakarya Zone show clear facies differences from north to south related to the northward subduction of the Neotethyan oceanic lithosphere (Yılmaz and Boztuğ, 1996; Şengör et al., 2003; Sipahi and Sadıklar, 2014). The block-faulted tectonic formation played a role in the settlement of granitoid in this magmatic arc (Gedikoğlu, 1978). The long axes of the granitoids being compatible with major tectonic fault directions (NE–SW and NW–SE) in the Black Sea region support the block tectonic formation. Granitoid in different geodynamic environments with various compositions and ages (Permo-Carboniferous to Eocene) has been described in the eastern Black Sea region (Moore et al., 1980; Sipahi, 1996, 2011, 2019; Sipahi and Sadıklar, 1996; Kaygusuz et al., 2012, 2014, 2016, 2020; Karslı et al., 2010; Sipahi et al., 2017, 2018, 2020, 2022, 2023; Dokuz and Sünnetçi, 2019). Upper Cretaceous granitoid rocks are dominant in the inner-arc environment of the eastern Sakarya Zone (Yılmaz and Boztuğ, 1996; Şengör et al., 2003; Sipahi et al., 2018). Granitoids in the region have low-K tholeiitic to calc-alkaline metaluminous and peraluminous properties (Karslı et al., 2010; Sipahi, 2011; Sipahi et al., 2018, 2022) and were formed during collisional, crustal thickening, and postcollisional regimes (Yılmaz and Boztuğ, 1996; Okay and Şahintürk, 1997; Boztuğ et al., 2003). The Early Cretaceous to Early Paleocene arc-related granitoids have calc-alkaline and metaluminous I-type characters (Okay and Şahintürk, 1997; Boztuğ et al., 2003; Sipahi et al., 2018). Zigana granitoid (Late Cretaceous, Kaygusuz et al., 2014), which is responsible for the contact metasomatism in the study area, is chemically of high-K calc-alkaline and metaluminous character and is composed of quartz monzonite, monzogranite, granite, and syenogranite (Figure 1b; Sipahi, 2011).

3. Magnetometric measurement method

Low-pass filtering, trend analysis, and upward analytical continuation are used to obtain long wavelengths in order to analyze the effects of deep masses, and high-pass filtering, downward analytical elongation, and second derivative analysis are used to obtain short wavelength changes in order to study the effects of near-surface masses (Yüzgül, 2010). The magnetic measurements obtained as a result of field studies must be corrected and interpreted. Land effects are usually minor and neglected unless the topography comprises steep slopes consisting of a high magnetic susceptibility substance (> 0.01 SI) (Sharma, 1997). In these studies, it is assumed that the underground masses are only magnetized by induction, and permanent magnetization is not considered in the interpretation studies (Sharma, 1997). Interpretations are done with two different methods, as direct and computing. The direct method is performed by evaluating data from the field. The interpretation of the graphs obtained from the distributions of the magnetic field anomalies corresponding to the measurement points provides a direct evaluation. For the computing, the deep analytic (downwards) continuation and upward continuation computing methods are used. In the deep analytic elongation method, the potential field data consists of the sum of an infinite number of sinusoidal waves (Griftin, 1949; Roy, 1966). The characteristic behavior of this sinusoidal wave at different harmonics carries information about the source of the potential field. These

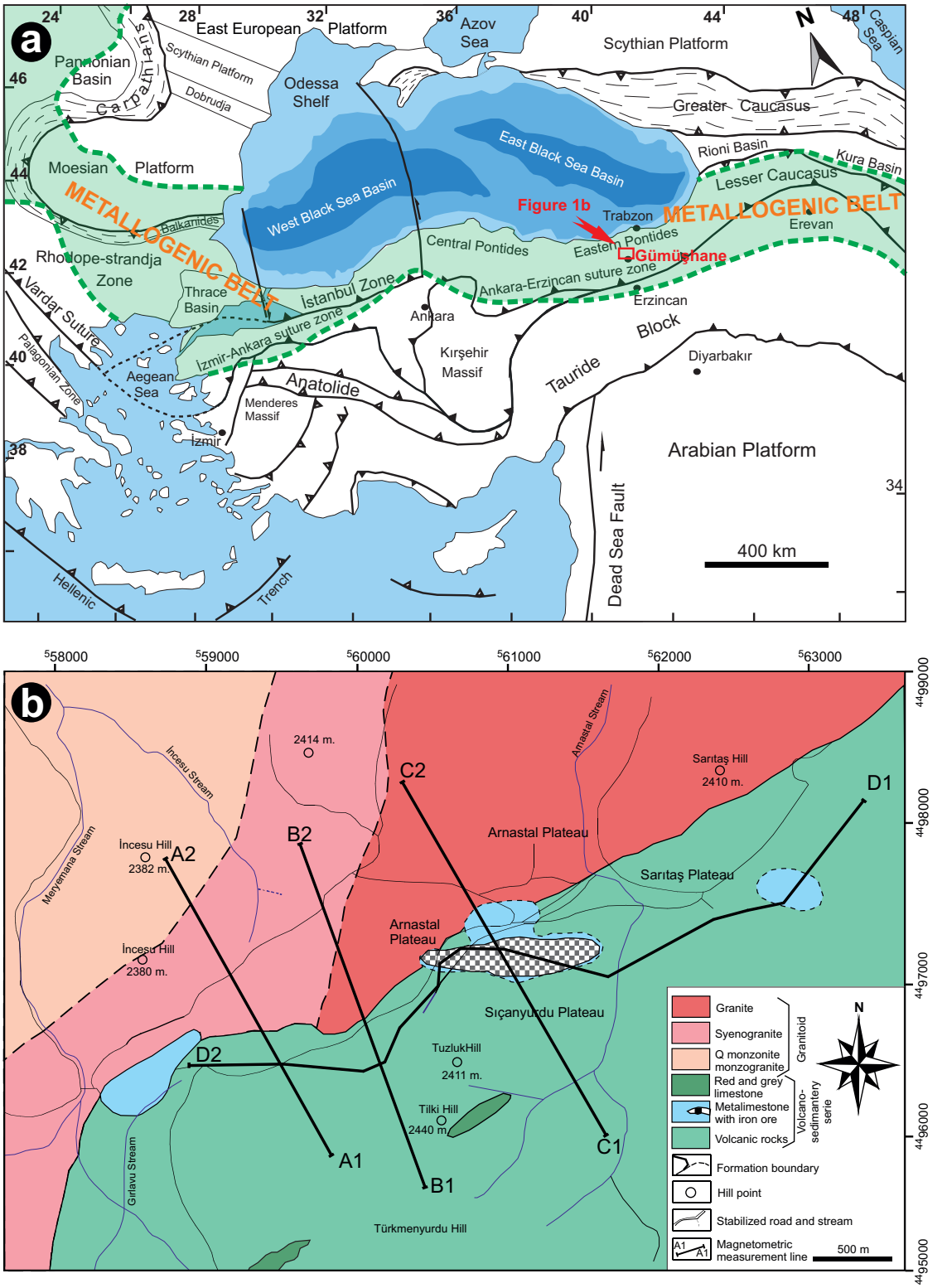

Figure 1. (a) Tectonic setting of Türkiye in relation to the Eurasian and Afro-Arabian platforms (Okay and Tüysüz, 1999) and (b) geological map of the study area (Sipahi, 2011).

information-bearing harmonics are determined at certain intervals. The small harmonic lengths mainly provide information about deep (regional) sources (Griftin, 1949; Roy, 1966). As the number of harmonics increases, i.e. the length of the harmonic increases, the effect of near-surface sources becomes apparent. The Fourier series is most commonly used to interpret these sinusoidal data (Roy, 1966). In the upward continuation computing method, the underground structures are divided into simple geological units and the corresponding magnetic signatures are then calculated. This process is continued by changing the physical dimensions and properties of the geological structure until the computed values are compatible with the data measured in the field.

The contribution of the magnetic field strength generated by the magnetic object to the measured value can be determined by measuring the magnetic susceptibility of the samples taken from this object. Susceptibility is the term used to describe the magnetic attribute that any material gains from a magnetic field. The ratio of the magnetic field inside of the material to the magnetic field outside of is a constant value. Magnetic susceptibility is a constant value that varies depending on the material's physical and chemical characteristics. It is defined in two ways: the volume susceptibility (k) calculated depending on the volume of the object and the mass susceptibility (x) calculated depending on the mass of the object (Ergin, 1985).

Two proton magnetometers and one susceptibility meter (MS-2 Bartington) were used during the current study. One of the magnetometers (IGS-2 proton magnetometer system) was used as the base station and the other (Elsec 820 proton magnetometer system) served as a rover unit. The sensitivity of both instruments was 0.1 gamma. The base station was generally built on the limestone. The time-domain change of the magnetic field was recorded every 5 min (Table S1). The magnetic susceptibility measurements were taken on the outcropped rocks using the field sensor (1×10^{-7} SI sensitivity).

The magnetic field intensity values recorded during the present study were plotted as a function of time. After diurnal correction, software with the potential field data processing was employed to grid the magnetic data and their upward continuation. Then, Surfer was used to create the total magnetic intensity (TMI) anomaly maps with reduction to the pole (RTP).

The processing software was an open-source program that includes a graphical user interface (GUI). This software was developed for processing, computing, and mapping of gravity and magnetic data by Arısoy and Dikmen (2011). Its most common application is spatial and frequency domain filtering of gravity and magnetic data.

4. Results

4.1. Rock types in the study area

Volcano-sedimentary series (Upper Cretaceous) and granitoid outcrops in the study area are shown in Figures 2a and 2b. The volcano-sedimentary series are cut by granitoid. The presence of soil and grass covering the land has obscured the clear delineation of rock contacts.

Volcano-sedimentary series: Volcanic rocks are dark and light grey andesite, quartz andesite, basalt, and their pyroclastics (autobrecciated andesite, agglomerate, and tuff) (Figure 2a). Secondary epidote, quartz, calcite, and chlorite are seen in these rocks. Macroscopically, pyrrhotite was detected in the cavities of the basalts. Basalt is fractured. Hematite fills the 5–15 cm-wide fractures of the basalt. The volcanic rocks display a microlitic porphyry texture and are composed of plagioclase (An_{26-50}), biotite (altered to chlorite) and accessory magnetite, and pyrrhotite. The secondary minerals are sericite, epidote, calcite, quartz, and chlorite (Figures 2c and 2d). Sedimentary rock is generally found as marl, sandy limestone, and limestone. The unit is in a northeast-southwest direction and dips approximately 30°– 45° towards the southwest. Moreover, red, and grey colored biomicrite (Upper Cretaceous; Sipahi, 1996, 2011) containing a thin layer of globotruncana fossils and light grey recrystallized limestone (Jurassic-Lower Cretaceous) as olistolith are also present in the volcano-sedimentary series.

The granitoid is light pink and dark and light gray in some places (Figure 2b). It is very fractured and weathered. Hematite and limonite occurrences are observed along the fractures of the granitoid. The granitoid has a macroscopically coarse, medium, and fine-grained texture, and quartz, plagioclase (An_{16-40}), orthoclase, biotite, hornblende, and clinopyroxene (augite) are also seen (Figures 2e and 2f). Apatite and sphene occur as an accessory. The granitoid is composed of quartz monzonite, monzogranite, granite, and syenogranite. Microscopically, the monzogranite is plagioclase, orthoclase, quartz, biotite, and hornblende, while the quartz monzonite is plagioclase, orthoclase, quartz, hornblende, biotite, and pyroxene, in decreasing abundance; the syenogranite is orthoclase, quartz, plagioclase, hornblende, biotite, and sphene, while the granite is quartz, orthoclase, plagioclase, hornblende, and biotite, in decreasing abundance. Epidote and chlorite are also common. The quartz monzonite has a more mafic composition of granite and syenogranite (Sipahi, 2011).

4.2. The Fe-skarn mineralization

Contact pyrometasomatic exoskarn mineralization occurred in between the limestone and granitoid at the Arnastal Plateau. The Fe-skarn mineralization between the limestone and the granitoid at the Arnastal Plateau is commonly fractured and distributed, and consists of limestone, skarn minerals, and ore (magnetite and specular hematite)

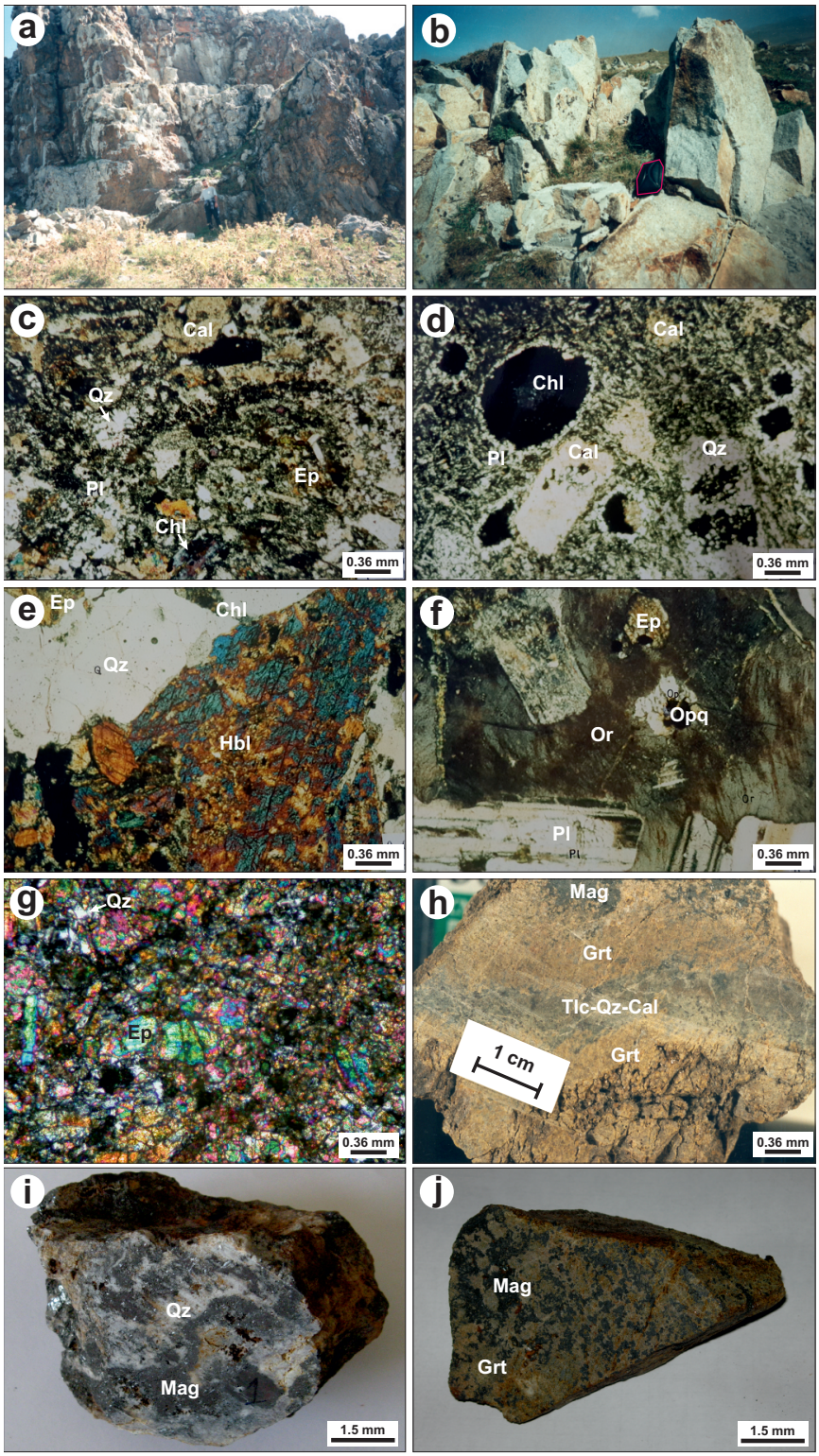

Figure 2. Field, rock, and mineral photographs from the study area. a) Basalt, b) granitoid, c) andesite tuff (sample no: 80, +N), d) basalt (sample no: 89, +N), e) granite in thin section (sample no: 42, +N), f) quartz monzonite in thin section (sample no: 34, >N), g) epidote in thin section, h) garnet, i) magnetite with quartz, and j) garnet with magnetite. Mineral abbreviations after Whitney and Evans (2010).

fragments. The Fe-skarn mineralization covers an area of approximately 100 × 50 m, and the ore fragments are approximately 1 × 0.5 and 1 × 1.5 m in size, massive, and less banding (Sipahi, 2011). The skarn mineral assemblages in the study area are composed of garnet (andradite), calcite, magnetite, epidote, actinolite, tremolite, quartz, hematite (specular), and, in lesser amounts, pyrrhotine and pyrite at the Arnastal Plateau, and clinopyroxene (diopside), ferri vesuvian, phlogopite at the Camiboğazı Plateau (Sipahi, 2011) (Figures 2g–2j). There is an average of 33.7% Fe in the Fe ore (Sipahi, 1996). Magnetite is generally massive and is sometimes banded (Figure 2i), spotted (Figure 2j), and fractured. It occurs together with hematite, which is generally specular in some samples. Hematite is the most common mineral after magnetite. Pyrite and pyrrhotite are seen less often (<0.1%).

4.3. Field study for magnetometry measurement

Based on the geological information previously obtained in the field, the magnetic survey was planned to be carried out on four lines that were determined according to the ore fragments seen on the surface and the contact between the granitoid and sedimentary-volcanic rocks. A geological cross-section is given in Figures 3a–3d for each line showing the types of rocks that were cut and where the measurements were taken.

The field geophysical survey included measurements of the earth's magnetic field and the magnetic susceptibility of the rocks. During this survey, the total components (t) of the magnetic fields were measured at intervals of 25 and/or 50 m along the four selected lines. Since most of the area was covered with recent sediments, surface susceptibility measurements were taken on the few available outcrops (Figure 3e). The first three (A1-A2, B1-B2, and C1-C2) magnetic measurement lines were made to determine the boundaries of the granite-volcano-sedimentary series, which constituted the ore hosting rocks and the basement, respectively, and the fourth (D1-D2) line was planned to determine the possible ore locations based on these first three lines, to delineate the boundaries of the rock units under the overlying material and reveal their changes with depth.

4.3.1. A1-A2 magnetic measurement line

Starting from the part where the andesite-basalt unit outcrops in the SE–NW direction, measurements were taken at intervals of 50 m, passing through the covered area to the granitoid outcrop. The magnetic field measurements, which began in the volcanic rocks and ended in the granitoid, were taken at 41 measurement points in total, with a length of 2000 m (Table S2). The surface susceptibility values measured from the outcropped rocks in the field were 1940 (10^{-7} SI) for basalt and 105 to 3946 (10^{-7} SI) for granite. The magnetic values corresponding to the susceptibility values of these rocks were 724.6 gamma for basalt and 201.7 to 395.1 gamma for granite, respectively. The magnetic field values in the covered area recorded on this line ranged from 23.1 to 865.7 gamma (Table S2, Figure 4a). Considering the two interpretation methods mentioned above, it was attempted to determine the approximate shapes and depths of the Fe-containing deposits and the boundaries of the geological units in the study area.

4.3.2. B1-B2 magnetic measurement line

A 2350-m-long magnetic survey was conducted in the NW–SE direction, approximately parallel to the A1-A2 line. A total of 47 measurements were taken at intervals of 50 m (Table S3). The surface susceptibility value measured on the basalt outcrop in the field was 122 (10^{-7} SI) and the magnetic value corresponding to the susceptibility value of this rock was 523.2 gamma. In general, it is noteworthy that there may be ore bodies between points 10 and 30, and 40 and 45 in the graph (Figure 4b). Magnetite ore can be found between these points in both massive and disseminated forms. In addition, by analyzing the shape of the peaks, an idea about the depths of the Fe ores can be provided (Figure 4b). The volcano-sedimentary series-granitoid boundary in the A1-A2 line was estimated as approximately 1–2 m at the edge and 2–5 m in the middle. As with the A1-A2 line, the volcano-sedimentary series-granite boundary under the covered part was thought to be at the same depth.

4.3.3. C1-C2 magnetic measurement line

This line was approximately parallel to the A1-A2 and B1-B2 lines. It had a length of 2600 m and consisted of 74 magnetic field readings performed from the SE to NW. Starting from the basaltic unit, magnetic measurements were taken towards the granitoid at intervals of 50 m for the first 23 points, at intervals of 25 m between points 23 and 64, and again at intervals of 50 m from point 64 onward (Table S4, Figure 4c). There was no outcrop rock in this line and the magnetic field values in the covered area ranged from – 97.7 to 1950 gamma. In the field, there was magnetite ore in the form of debris in the middle part of the C1-C2 line. There was also limestone in the form of small outcrops in this area.

4.3.4. D1-D2 magnetic measurement line

To determine the ore, measurements on the D1-D2 line were taken on the possible volcano-sedimentary series-granite boundaries along the dashed lines. A total of 206 magnetic readings located at intervals of 25 m were taken over 5125 m in the NE–SW direction (Table S5, Figure 4d). The surface susceptibility values measured from the outcropped rocks in this line were 1 to 34 (10^{-7} SI) for limestone, 78 to 3750 (10^{-7} SI) for basalt, and 219 to 745 (10^{-7} SI) for granite. The magnetic values corresponding to the susceptibility values of these rocks were 808 to 990.7 gamma on the limestone, 874 to 876.4 gamma on the ba-

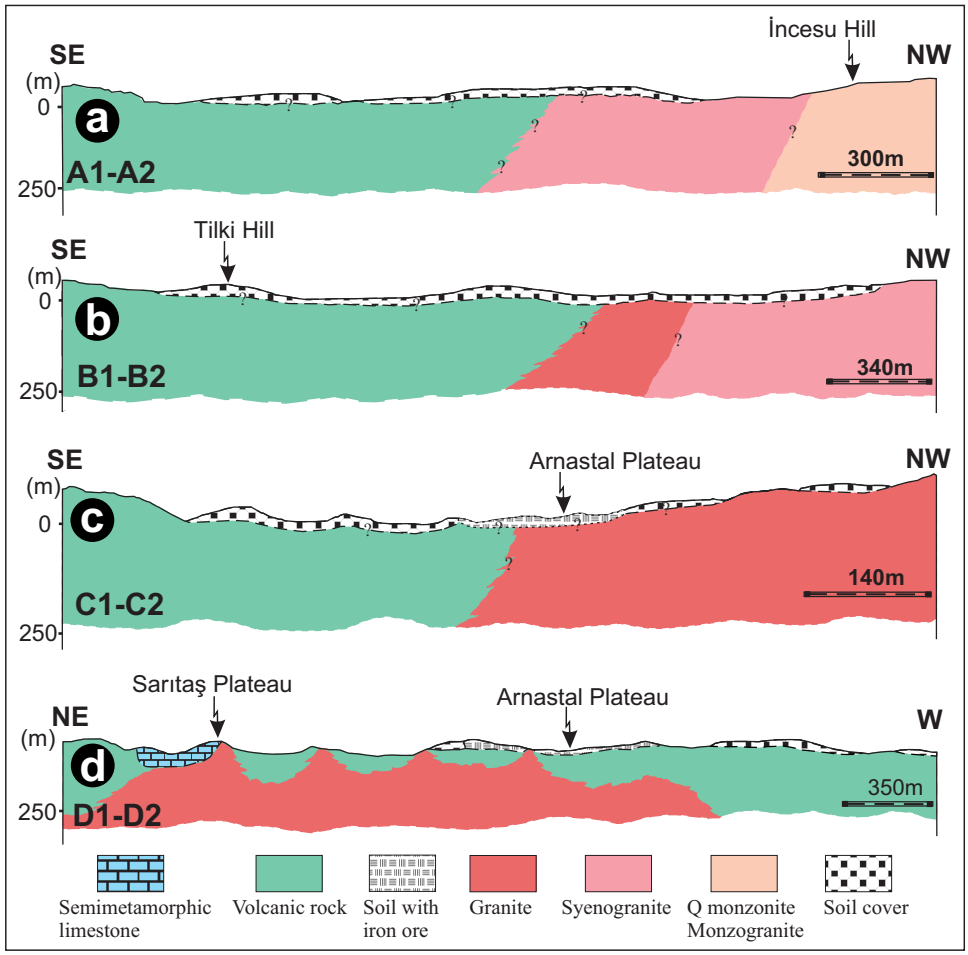

Figure 3. a–d) Geological cross-sections of the four magnetic measurement lines and e) measurement with a susceptibility instrument on outcrops in the field.

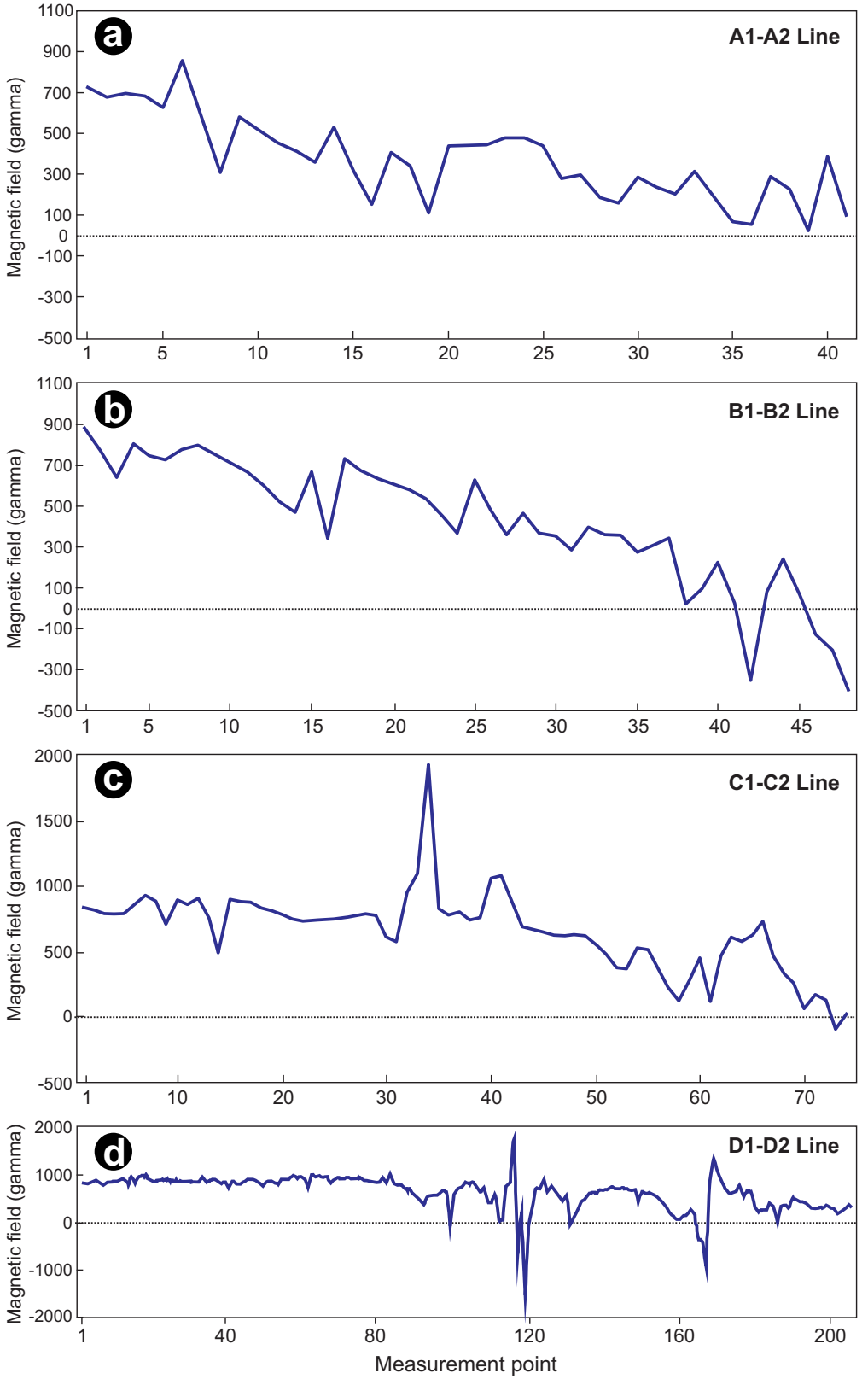

Figure 4. Graphics of the magnetic field anomaly values measured along the lines.

salt, and 725.8 to 910.1 gamma on the granite, respectively. The magnetic field values in the covered area ranged from 1344 to 26.5 gamma.

5. Discussion

In the evaluation of earth magnetic field data, it is aimed to determine parameters such as the horizontal positions, depths, and geometrical properties of underground structures that cause magnetic anomalies (Adagunodo et al., 2015; Öksüm and Dolmaz, 2018). Gravity and magnetic techniques are potential field methods of natural origin, and their data are processed using similar techniques. In magnetic computing, changes in the magnetic field on the surface as a result of masses/ore or rocks with different magnetic susceptibilities (magnetite, ilmenite, hematite, granodiorite, granite, basalt, limestone, etc.) underground are measured. High values obtained after some corrections are applied to the measurements taken on the earth, such as the sum of shallow (residual) and deep structural (regional) effects. Depending on the purpose of the study, shallow effects are excluded if a deeper and regional structure is focused on, and deep effects are excluded from the anomaly if the aim is to investigate local effects near the surface.

In this study, the TMI and its upward continuation anomaly maps were created using the magnetic values of the A1-A2, B1-B2, and C1-C2 lines from 1996 magnetic measurement data (Tables S2–S4). International geomagnetic reference field values of the Arnastal Plateau locality in 1996 were calculated[1] and an RTP anomaly map was drawn (Figures 5 and 6). Indeed, the TMI values with the RTP were upward and continued to heights of 50, 100, and 200 m, which gave high contrasts compatible with skarn mineralization, and possible skarn mass anomalies that varied depending on depth were revealed (Figure 6). Moreover, the calculation of the first vertical deriva-

[1]NOAA (2023). Magnetic Field Calculators [online]. Website https://www.ngdc.noaa.gov/geomag/calculators/magcalc.shtml?useFullSite=true [accessed 01-30 June 2023].

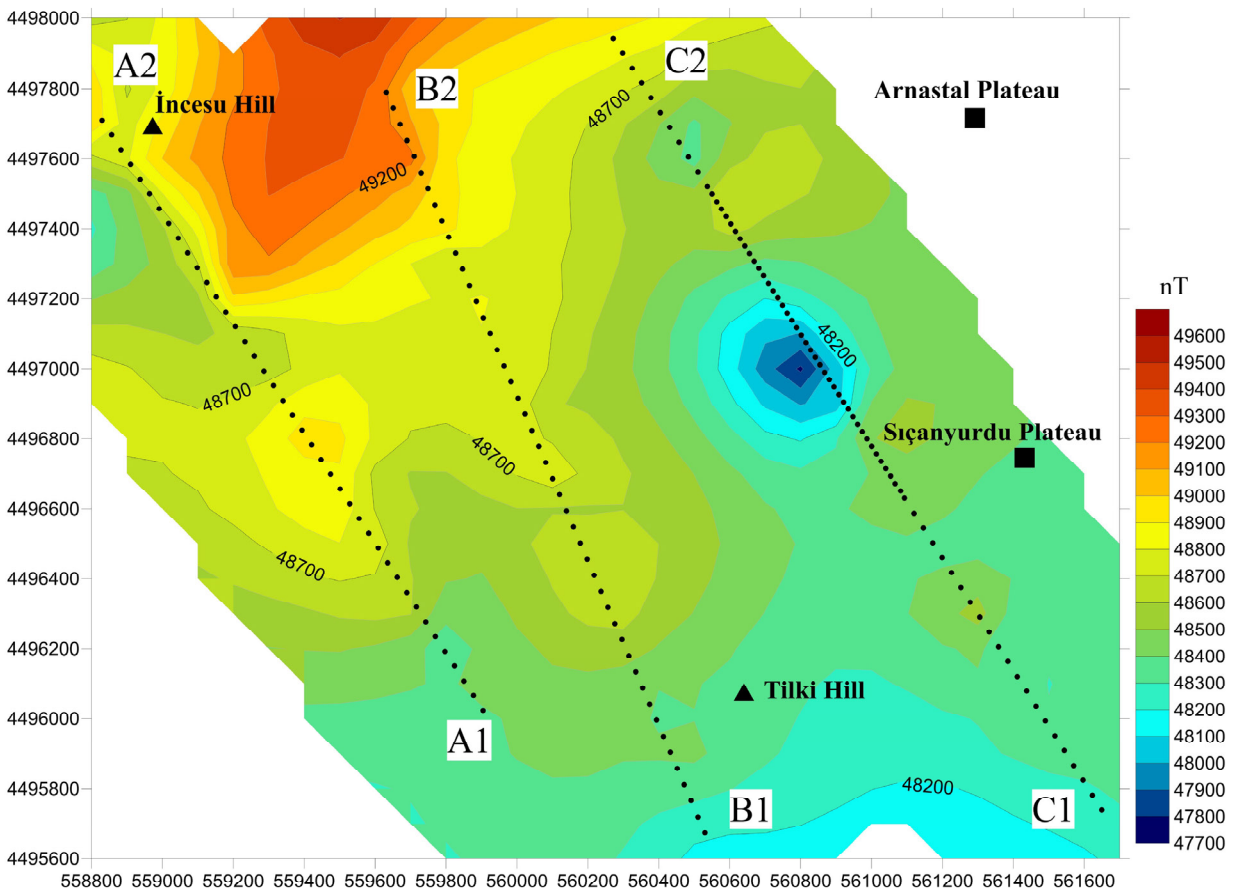

Figure 5. RTP anomaly map.

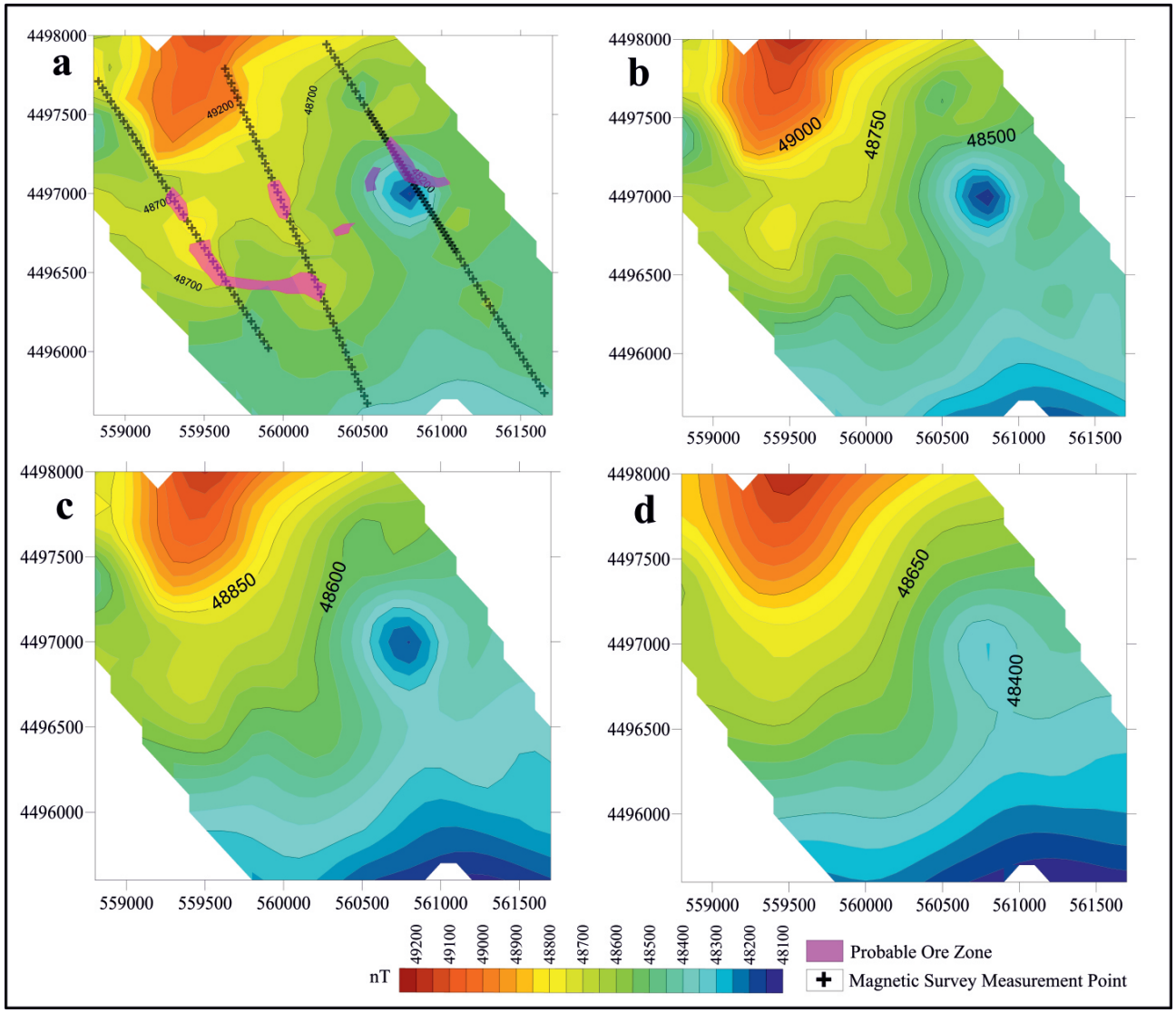

Figure 6. a) RTP anomaly map with probable ore mineralization, b) 50 m upward analytical extension anomaly map, c) 100 m upward analytical extension anomaly map, and d) 200 m upward analytical extension anomaly map.

tive (VD) and the tilt derivative (TDR) of this map made it possible to perform detailed mapping of the subsurface magnetic sources (Figure 7).

5.1. A1-A2 magnetic measurement line

It is believed that there are three separate Fe ore-containing units with high susceptibility at a depth of about 50 m in limestone with low susceptibility in the volcano-sedimentary series. The low-susceptibility environment is thought to be composed of limestone or impure marble containing scattering Fe ore. In addition, the very small periodic changes in the magnetic value in the covered area indicated the presence of ores in the form of scattering and small masses in the silicified parts of the limestone. A RTP profile was added above the interpreted section and the possible geological section extracted based on the interpretation methods is given in Figure 8a.

5.2. B1-B2 magnetic measurement line

When the graph in Figure 8b was examined, there were masses with high magnetite content between points 10 and 15, 25 and 30, and 40 and 45. Based on two interpretation techniques, it is believed that the surface cover unit started at a depth of approximately 1–2 m at the edges and ranged to a depth of 2–5 m in the middle (Figure 8b).

5.3. C1-C2 magnetic measurement line

According to both the direct interpretation of the magnetic data and the deep analytical extension method, one mass was

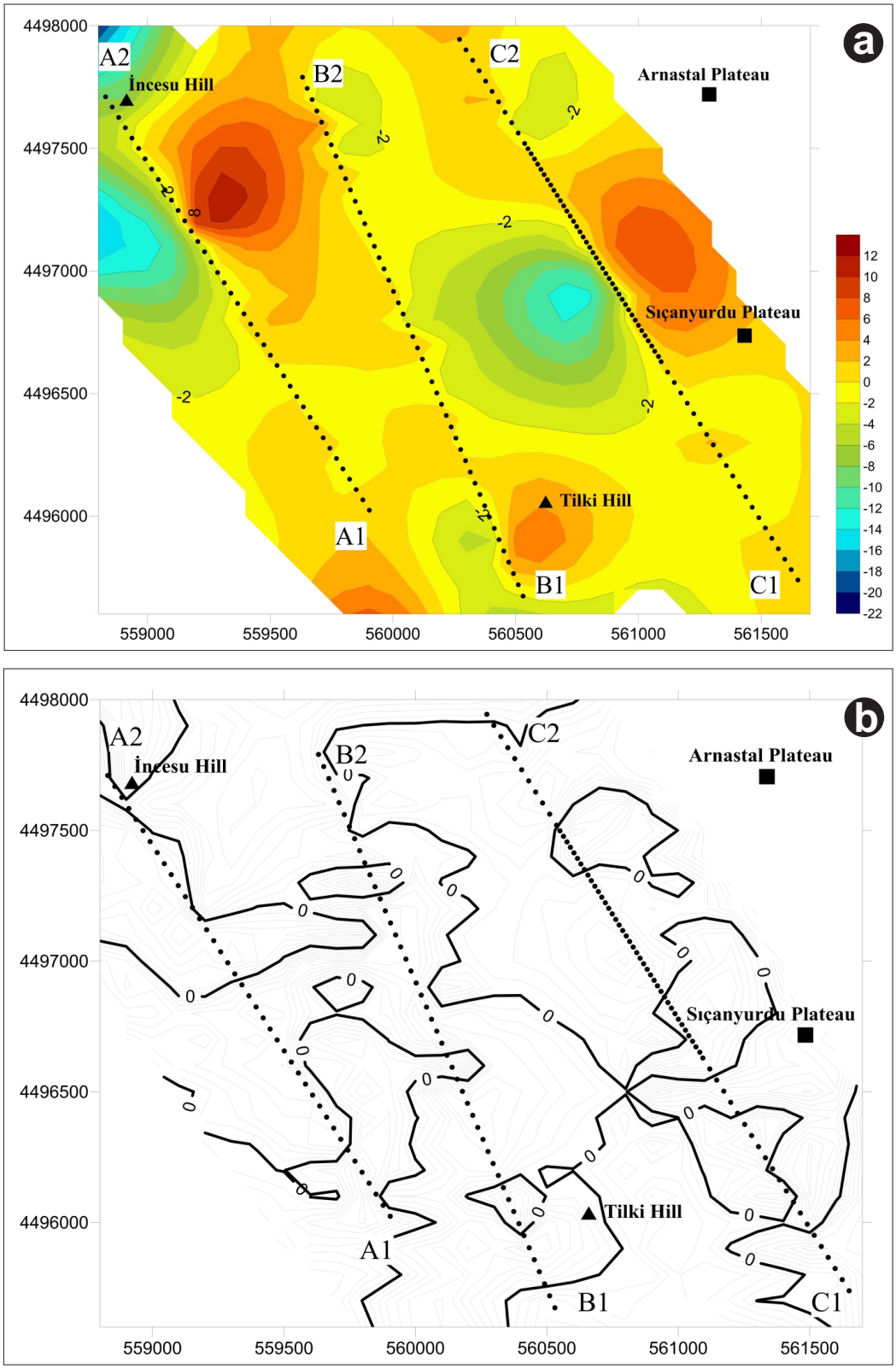

Figure 7. a) VD map and b) TDR map.

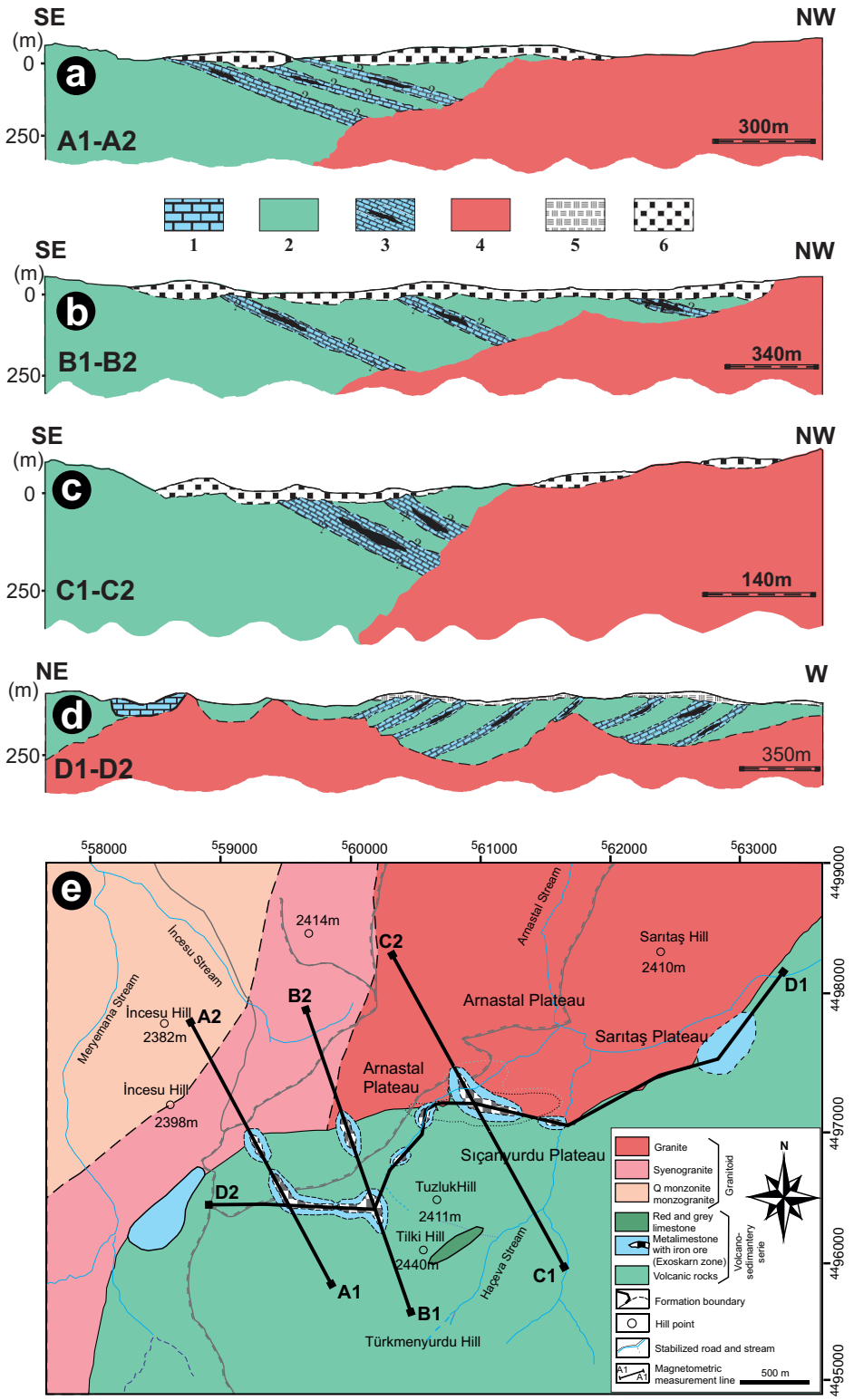

Figure 8. (a–d) Geological sections obtained with the interpretation of the magnetic measurement values of lines A1-A2, B1-B2, C1-C2, and D1-D2 (1: semimetamorphic limestone, 2: volcanic rock, 3: Fe ore in the limestone, 4: granite, 5: soil cover with little Fe ore, 6: soil cover). (e) Geological map obtained via interpretation of the geology and magnetic anomalies.

located with a high Fe content (Figure 8c) at point 31 and a smaller Fe ore was located a little deeper at point 40. Both of the Fe masses were located in limestone with low susceptibility.

5.4. D1-D2 magnetic measurement line

As a result of the interpretation of the magnetic measurements, ore bodies of various sizes were detected in the covered area. Based on the interpretation techniques, granitic rocks with higher susceptibility began at a depth of approximately 275 m and were observed as the basement rock in this line (Figure 8d). The granite formed a border with the volcano-sedimentary series with a highly fluctuating pattern at its depth. It outcropped from place to place in a small area in the east of Sarıtaş Plateau. The presence of limestone between points 74 and 119, 122 and 145, and 148 and 207 was determined from the magnetic measurements. Within the limestone, there were masses with a high Fe content and variable sizes. In general, the parts where possible mineralization was observed were in the limestone and in the granite-limestone contact in the study area (Figure 8d).

6. Coevaluation of the magnetic lines

When the surface susceptibility values measured from the rocks in the field were examined, it was the lowest (1 – 34 × 10^{-7} SI) in the limestone, high (78 – 1940 × 10^{-7} SI) in the volcanic unit, and very high (693 – 3040 × 10^{-7} SI) in the granitoid. This change in the susceptibility values reflects the alteration (physical or chemical) of the rocks, their homogeneity, and the mineralogy. The ore assumed in the four magnetic lines may be in the form of scattering or may have developed in the form of lenses. In the parts where this magnetic mineralization was observed, magnetic mineralization in the surface cover material was determined both in the interpretation and in the field. However, an ore stack in the form of debris was not reflected in the interpretation section. It was attempted to determine the possible ore and formation boundaries by processing the data of these four magnetic lines on geological maps (Figure 8e). Thus, the current geological map was developed via magnetic computing (Figure 8e).

The presence of a lithological trend in the north-east and south-west was observed in the TMI anomaly map with RTP obtained as a result of the magnetic measurements. It was determined that a low magnetic field corridor in a narrow area in the north of the Tilki Tepe, west and northwest of the Sıçanyurdu Plateau, and south of the Arnastal Plateau was compatible with the limestone-granite contacts, which is a potential field in terms of the skarn mineralization. As a result of an upward analytical extension, it was determined that the contacts of the mass anomalies due to possible granites and volcanics were very close to the surface. This revealed the conclusion that the narrow magnetic field anomalies, which were compatible with smaller limestone blocks in terms of volume, had no continuity toward the deeper areas.

7. Conclusion

Fe-skarn mineralization was found as exoskarn around the Sarıtaş and Arnastal plateaus (Gümüşhane, Türkiye) as fragments and the field was covered with plants (grasses, flowers, etc.). Magnetic computing was applied for the first time in the study area to investigate the continuity of the Fe-skarn mineralization under the ground, because the size and spread of the Fe-skarn type mineralization seen in fragments in the Arnastal Plateau could not be fully determined with geological studies.

The units commonly seen in the study area are volcano-sedimentary series (Upper Cretaceous) and granitoids. Limestone, sandy limestone, marl, andesite, quartz andesite, basalt and their pyroclastics occur in the volcano-sedimentary series. This series includes a thin layer of the red limestone (Upper Cretaceous) and olistolith recrystallized limestones (Jurassic-Lower Cretaceous). Granitoid (quartz monzonite, syenogranite, granite, and monzogranite as a result of modal composition) intrudes into all of these rocks.

Mineral paragenesis of the contact pyrometasomatic exoskarn mineralization occurring in between the limestone and granitoid in the Arnastal Plateau are ferric vesuvian, boron phlogopite, andradite, calcite, actinolite, tremolite, epidote, quartz, magnetite, hematite, pyrrhotite, and pyrite minerals.

To determine the possible boundaries of the units in the field, their possible geological sections were drawn, and the possible locations of the Fe ore bodies were examined using the magnetic method. The surface susceptibility data measured from the studied rocks showed that it was the lowest (1 – 34 × 10^{-7} SI) in the limestone, high (78 – 1940 × 10^{-7} SI) in the volcanic rock, and very high (693 – 3040 × 10^{-7} SI) in the granitoid. This change in the susceptibility values points to the alteration (physical or chemical) of the rocks, their homogeneity, and the lack or presence of Fe minerals. The magnetic research was conducted along a study area measuring 12,075 m long with 25 and/or 50 m station spacing. Based on the computation of the magnetic data, it was determined that there may be Fe ore bodies in eight places between the Sarıtaş and Kurtdere plateaus. These Fe ore mineralizations or bodies could be within the limestones and could be scattered and lenticular at a depth of about 15–25 m from the surface.

Acknowledgment

This study was taken from a section of the first author's MSc thesis. The authors thank Emin Sipahi, Hakan Karslı (Karadeniz Technical University), and Saliha Topçuoğlu (MTA, Trabzon) for their support in the magnetic mea-

surement field studies and acknowledge the financial support of Karadeniz Technical University (Project No: 96.112.005.10). Moreover, the first author gives special thanks to Birsengül Sipahi. We gratefully acknowledge Dr. Namık Aysal's editorial remarks as well as the reviews of Dr. Mualla Cengiz and the two anonymous referees.

References

Adagunodo TA, Sunmonu LA, Adeniji AA (2015). An overview of magnetic method in mineral exploration. Journal of Global Ecology and Environment 3 (1): 13-28.

Arısoy MÖ, Dikmen Ü (2011). Potensoft: MATLAB-based software for potential field data processing, modeling and mapping. Computers and Geosciences 37 (7): 935-942. https://doi.org/10.1016/j.cageo.2011.02.008

Aydın A (1994). Bayburt-Saruhan skarn zonunun süseptibilite ve manyetik ölçümleri ile değerlendirilmesi. MSc thesis, Karadeniz Technical University, Trabzon, Türkiye (in Turkish).

Aydın A, Ferré EC, Aslan Z (2007). The magnetic susceptibility of granitic rocks as a proxy for geochemical composition: Example from the Saruhan granitoids, NE Turkey. Tectonophysics 441: 85-95. https://doi.org/10.1016/j.tecto.2007.04.009

Aydın A, Sipahi F, Karslı H, Gelişli K, Kadirov F (1997). Interpretation of magnetic anomalies on covered fields using normalized full gradient method. International Geoscience Conference and Exhibition Book 15, p. 18.

Bilim F, Ateş A (2003). Analytic signal inferred from reduced to the pole data. Journal of the Balkan Geophysical Society 6: 66-74.

Boztuğ D, Kuşçu I, Erçin AI, Avcı N, Şahin SY (2003). Mineral deposits associated with the pre-, syn- and postcollisional granitoids of the neo-Tethyan convergence system between the Eurasian and Anatolian plates in NE and Central Turkey. In: Eliopoulos D (editor). Mineral Exploration and Sustainable Development. Rotterdam, The Netherlands: Millpress Science Publishers, pp. 1141-1144.

Büyüksaraç A, Jordanova D, Ateş A, Karloukovski V (2005). Interpretation of the gravity and magnetic anomalies of the Cappadocia region, central Turkey. Pure and Applied Geophysics 162: 2197-2213. https://doi.org/10.1007/s00024-005-2712-9

Çinku MC, Rammlmair D, Hisarlı MZ, Orbay N (2009). A combined rock magnetic and geochemical investigation of Upper Cretaceous volcanic rocks in the Pontides, Turkey. Studia Geophysica et Geodaetica 53: 475–495. https://doi.org/10.1007/s11200-009-0035-5

Çinku MC, Hisarlı MZ, Hirt AM, Heller F, Ustaömer T et al. (2015). Evidence of late cretaceous oroclinal bending in north-central Anatolia: Paleomagnetic results from Mesozoic and Cenozoic rocks along the Izmir-Ankara-Erzincan Suture Zone. Geological Society London Special Publications 425: 189-212, https://doi.org/10.1144/SP425.2

Çinku MC, Hisarli ZM, Heller F, Orbay N, Ustaömer T (2011). Middle Eocene paleomagnetic data from the eastern Sakarya Zone and the central Pontides: implications for the tectonic evolution of north central Anatolia. Tectonics 30 (1). https://doi.org/10.1029/2010TC002705

Çinku MC, Ustaömer T, Hirt AM, Hisarli ZM, Heller F et al. (2010a). Southward migration of arc magmatism during latest Cretaceous associated with slab-steepening, East Pontides, N Turkey: new paleomagnetic data from the Amasya region. Physics of the Earth and Planetary Interiors 182 (1–2): 18-29. https://doi.org/10.1016/j.pepi.2010.06.003

Çinku MC (2010b). Paleogeographic evidence on the Jurassic tectonic history of the Pontides: New paleomagnetic data from the Sakarya continent and Eastern Pontides. International Journal of Earth Sciences 100: 1633-1645. https://doi.org/10.1007/s00531-010-0569-3

Cengiz M (2023). Palaeomagnetic evidence of the deformation of the Pontides during the closure of the Intra-Pontide Ocean in the early Cretaceous. Geophysical Journal International 234 (3): 1835-1854. https://doi.org/10.1093/gji/ggad167

Dixon JC, Pereira J (1974). Plate Tectonics and mineralization in the Tethyan region. Mineralium Deposita 9: 185-198. https://doi.org/10.1007/BF00203995

Dokuz A, Sünnetçi K (2019). Jurassic acidic magmatism in a back-arc setting, eastern Sakarya Zone, Turkey: Geochemical constraints and an evolutionary model. Lithos 332–333: 312-327. https://doi.org/10.1016/j.lithos.2019.02.022

Elmas A, Babacan AE (2021). Manyetik özellik gösteren gömülü bir cismin sınır analizi ve NTG yöntemleriyle konumunun belirlenmesi. Adıyaman Üniversitesi Mühendislik Bilimleri Dergisi 8: 196-202 (in Turkish).

Ergin K (1985). Uygulamalı Jeofizik, İTÜ Maden Fakültesi, İstanbul (in Turkish).

Gedikoğlu A (1978). Harşit granit karmaşığı ve çevre kayaçları. Doçentlik Tezi, Karadeniz Technical University, Trabzon, Türkiye (in Turkish).

Griftin WR (1949). Residual gravity theory and practice. Geophysics 14 (1): 38-58. https://doi.org/10.1190/1.1437506

Haidarian Shahri MR, Karimpour MH, Malekzadeh A (2010). The exploration of gold by magnetic method in Hired Area South Khorasan, a case study. Journal of the Earth and Space Physics 35 (4): 33-44.

Ishihara S (1977). The magnetite-series and ilmenite-series granitic rocks. Mining Geology 27: 293-305. https://doi.org/10.11456/shigenchishitsu1951.27.293

Ishihara S, Hashimoto M, Machida M (2000). Magnetite/ilmenite-series classification and magnetic susceptibility of the Mesozoic-Cenozoic batholiths in Peru. Resource Geology 50: 123-129. https://doi.org/10.1111/j.1751-3928.2000.tb00062.x

Karslı O, Dokuz A, Uysal İ, Aydın F, Chen B et al. (2010). Relative contributions of crust and mantle to generation of Campanian high-K calc-alkaline I-type granitoids in a subduction setting, with special reference to the Harşit Pluton, Eastern Turkey. Contributions to Mineralogy and Petrology 160: 467-487. https://doi.org/10.1007/s00410-010-0489-z

Kaygusuz A, Arslan M, Siebel W, Sipahi F, İlbeyli N (2012). Geochronological evidence and tectonic significance of Carboniferous magmatism in the southwest Trabzon area, eastern Pontides, Turkey. International Geology Review 54 (15): 1776-1800. https://doi.org/10.1080/00206814.2012.676371

Kaygusuz A, Arslan M, Siebel W, Sipahi F, İlbeyli N et al. (2014). LA-ICP MS zircon dating, whole-rock and Sr-Nd-Pb-O isotope geochemistry of the Camiboğazı pluton, Eastern Pontides, NE Turkey: Implications for lithospheric mantle and lower crustal sources in arc-related I-type magmatism. Lithos 192-195: 271-290. https://doi.org/10.1016/j.lithos.2014.02.014

Kaygusuz A, Arslan M, Sipahi F, Temizel İ (2016). U-Pb zircon chronology and petrogenesis of carboniferous plutons in the northern part of the Eastern Pontides, NE Turkey: Constraints for Paleozoic magmatism and geodynamic evolution. Gondwana Research 39: 327-346. https://doi.org/10.1016/j.gr.2016.01.011

Kaygusuz A, Yücel C, Arslan M, Temizel İ, Yi K et al. (2020). Eocene I-type magmatism in the Eastern Pontides, NE Turkey: Insights into magma genesis and magma-tectonic evolution from whole-rock geochemistry, geochronology and isotope systematics. International Geology Review 62 (11): 1406-1432. https://doi.org/10.1080/00206814.2019.1647468

Meijers MJM, Kaymakci N, van Hinsbergen DJJ, Langereis CG, Stephenson RA et al. (2010). Late cretaceous to Paleocene oroclinal bending in the central Pontides (Turkey). Tectonics 29 (4). https://doi.org/10.1029/2009TC002620

Mekkawi MM (2012). Application of magnetic method in mineral exploration: iron ore deposit, south zagros suture zone, Iraq. Egyptian Geophysical Society EGS Journal 10 (1): 117-124.

Moore WJ, McKee EH, Akıncı Ö (1980). Chemistry and chronology of plutonic rocks in the Pontide mountains, northern Turkey. Symposium of European Copper Deposits, Belgrade, pp. 209-216.

Navaanchimed A, Khuut T, Turtogtokh B, Sengee M, Purev D et al. (2015). Geophysical exploration for skarn-type iron deposits in western Mongolia. Proceedings of the 12th SEGJ International Symposium, pp. 221-223.

Okay AI, Şahintürk Ö (1997). Geology of the Eastern Pontides. In: Robinson AG (editor). Regional and petroleum geology of the Black Sea and surrounding region. AAPG Memoir 68: 292-311.

Okay AI, Tüysüz O (1999). Tethyan sutures of northern Turkey. The Mediterranean basin: tertiary extension within the Alpine orogeny. Geological Society, London, Special Publications 156: 475-515. https://doi.org/10.1144/GSL.SP.1999.156.01.22

Öksüm E, Dolmaz MN (2018). Estimation of the depth and geometry of simple shaped subsurface magnetic structures causing magnetic anomalies based on analytical signal technique. Süleyman Demirel Üniversitesi Fen Bilimleri Enstitüsü Dergisi 22 (2): 993-997 (in Turkish with an abstract in English). https://doi.org/10.19113/sdufbed.24814

Pandarinath K, Rivas-Hernandez JL, Arriaga-Fuentes JA, Yanez-Davila D, Gonzalez-Partida E et al. (2023). Hydrothermal alteration of surficial rocks at Los Humeros geothermal field, Mexico: a magnetic susceptibility approach. Arabian Journal of Geosciences 16: 259. https://doi.org/10.1007/s12517-023-11306-3

Pandarinath K, Shankar R, Torres-Alvarado IS, Warrier AK (2014). Magnetic susceptibility of volcanic rocks in geothermal areas: Application potential in geothermal exploration studies for identification of rocks and zones of hydrothermal alteration. Arabian Journal of Geosciences 7: 2851-2860. https://doi.org/10.1007/s12517-013-1013-3

Pandarinath K, Shankar R, Santoyo E, Shwetha S, García-Soto AY et al. (2019). A rock magnetic fingerprint of hydrothermal alteration in volcanic rocks - An example from the Los Azufres Geothermal Field, Mexico. Journal of South American Earth Sciences 91: 260-271. https://doi.org/10.1016/j.jsames.2019.02.018

Roy A (1966). The method of continuation in mining geophysical interpretation. Geoexploration 4 (2): 65-83. https://doi.org/10.1016/0016-7142(66)90012-3

Sharma PV (1997). Environmental and engineering geophysics. Cambridge University Press.

Sipahi F (1996). Camiboğazı ve Sarıtaş Yaylaları arasındaki bölgenin petrografi ve maden yatakları açısından incelenmesi. MSc Thesis, Karadeniz Technical University, Trabzon, Türkiye (in Turkish).

Sipahi F (2011). Formation of skarns at Gümüşhane (Northeastern Turkey). Neues Jahrbuch für Mineralogie-Abhandlungen 188 (2): 169-190. https://doi.org/10.1127/0077-7757/2011/0199

Sipahi F (2019). Nature of the tourmaline in quartz porphyry in the E Sakarya zone (NE Turkey): geochemistry and isotopic approach. Periodico di Mineralogica 88 (3): 333-351. https://doi.org/10.2451/2019PM859

Sipahi F, Sadıklar MB (1996). Kontaktmetasomatische vererzungen von Arnastal Yayla (Gümüşhane, NE-Türkei). Eur J Mineralogist, Kiel - Deutschland, Abstract 8 (1): 267 (in German).

Sipahi F, Sadıklar MB (2014). Geochemistry of dacitic volcanics in the Eastern Pontides (NE Turkey). Geochemistry International 4: 329-49. https://doi.org/10.7868/S0016752514040086

Sipahi F, Akpınar İ, Saydam Eker Ç, Kaygusuz A, Vural A et al. (2017). Formation of the Eğrikar (Gümüşhane) Fe–Cu skarn type mineralization in NE Turkey: U–Pb zircon age, lithogeochemistry, mineral chemistry, fluid inclusion, and O-H-C-S isotopic compositions. Journal of Geochemical Exploration 182 (Part A): 32-52. https://doi.org/10.1016/j.gexplo.2017.08.006

Sipahi F, Gücer MA, Dokuz A, Yi K, Kaygusuz A et al. (2023). The Sr, Nd, Pb and Hf isotopes and crystallization conditions of the middle Eocene Dağdibi Pluton in the eastern Sakarya Zone, Turkey. Geological Magazine 160: 1193-1210. https://doi.org/10.1017/S001675682300033X

Sipahi F, Gücer MA, Saydam Eker Ç (2020) Geochemical composition of magnetite from different iron skarn mineralizations in NE Turkey: implication for source of ore forming fluids. Arabian Journal of Geosciences 13 (2): 70. https://doi.org/10.1007/s12517-019-5052-2

Sipahi F, Kaygusuz A, Saydam Eker Ç, Vural A, Akpınar İ (2018). Late Cretaceous arc igneous activity: the Eğrikar Monzogranite example. International Geology Review 60 (3): 382-400. https://doi.org/10.1080/00206814.2017.1336120

Sipahi F, Saydam Eker Ç, Akpınar İ, Gücer MA, Vural A et al. (2022). Eocene magmatism and associated Fe-Cu mineralization in northeastern Turkey: a case study of the Karadağ skarn. International Geology Review 64 (11): 1530-1555. https://doi.org/10.1080/00206814.2021.1941323

Şengör AMC, Özeren S, Genç T, Zor E (2003). East Anatolian high plateau as a mantle-supported, north-south shortened domal structure. Geophysical Research Letters 30, 8045. https://doi.org/10.1029/2003GL017858

Şengör AMC, Yılmaz Y (1981). Tethyan evolution of Turkey: a plate tectonic approach. Techtonophysics 75: 181-241. https://doi.org/10.1016/0040-1951(81)90275-4

Villaseca C, Ruíz-Martínez VC, Pérez-Soba C (2017). Magnetic susceptibility of Variscan granite-types of the Spanish Central System and the redox state of magma. Geologica Acta 15 (4): 379-394. https://doi.org/10.1344/GeologicaActa2017.15.4.8

Vincent A, Kassim M, Charles M, Willis A, Gerald M (2013). Geophysical exploration of iron ore deposit in Kimachia area in Meru County in Kenya, using gravity and magnetic techniques. International Journal of Science and Research 2 (11): 104-108. https://www.ijsr.net/getabstract.php?paperid=02013314

Whitney DL, Evans BW (2010). Abbreviations for names of rock-forming minerals. American Mineralogist 95: 185-187. https://doi.org/10.2138/am.2010.3371

Yılmaz S, Boztuğ D (1996). Space and time relations of three plutonic phases in the Eastern Pontides, Turkey. International Geology Review 38: 935-956. https://doi.org/10.1080/00206819709465373

Yüzgül S (2010). Eskişehir Grabeni'nin potansiyel alan verileri (gravite ve manyetik) ile araştırılması ve yorumu. MSc Thesis, Dokuz Eylül University, İzmir, Türkiye (in Turkish).

Table S1. Example of the magnetic measurement values measured at the base station at different time intervals.

Base field: 47000								Measuring range: 5 min		
Line: 0 Grid: 0										
Station: 0		Explanations (Difference between readings)								
Time	Magnetic field	+ 1	+ 2	+ 3	+ 4	+ 5	+ 6	+ 7	+ 8	+ 9
10:19:50	49084.8	−8.9	−1.0	0.0	−1.0	−21.0	17.4	−0.7	−0.4	−5.0
11:09:50	49065.7	−3.9	−0.2	−0.2	−0.3	−1.7	−0.7	7.1	−0.1	−3.0
11:59:50	49063.4	2.2	−0.5	−9.4	−0.7	0.8	0.6	1.2	2.8	2.0
12:49:50	49064.4	0.1	7.0	−10.4	0.0	1.9	0.6	−0.8	0.4	9.0
13:39:50	49073.0	0.9	0.5	0.9	−0.6	0.2	0.2	0.2	2.0	2.0
14:29:50	49079.8	0.9	2.4	−1.3	0.7	−0.3	−0.8	−1.3	0.4	0.0
15:19:50	49080.7	10.5	−10.7	1.0	−4.4	−0.6	1.8	13.0	−4.7	0.0
16:09:50	49086.6	4.4	−3.6	1.4	−0.8	3.1	0.0	0.9	0.3	−6.0
16:59:50	49086.8	0.7	0.8	−0.3	−1.7	−3.2	0.5	3.1	1.9	−0.0
17:49:50	49088.1	−0.4	−0.7	−0.5	−0.6	−0.6	0.2	−0.3	−0.5	−0.0
18:39:50	49083.4	0.6	0.2	1.4	−0.2	−0.9	1.7	−1.5	−1.0	−1.0

Table S2. Values for to the A1-A2 magnetic measurement line.

Point	Horizontal scale (m)	Time	TMI	Magnetic field base value	Magnetic field anomaly	Susceptibility	Rock unit
1	0	10:59	48359.8	49084.4	724.6	1940	Basalt
2	50	11:01	48405.2	49084.4	679.2		Soil cover
3	100	11:03	48383.2	49079.8	696.6		Soil cover
4	150	11:04	48397.4	49079.8	682.4		Soil cover
5	200	11:05	48455.4	49079.8	624.4		Soil cover
6	250	11:07	48200	49065.7	865.7		Soil cover
7	300	11:10	48488.5	49065.7	577.2		Soil cover
8	350	11:15	48757	49061.8	304.8		Soil cover
9	400	11:16	48480.7	49061.8	581.1		Soil cover
10	450	11:17	48545.2	49065.5	520.3		Soil cover
11	500	11:18	48608.4	49065.5	457.1		Soil cover
12	550	11:20	48652.3	49065.5	413.2		Soil cover
13	600	11:22	48704.3	49065.5	361.2		Soil cover
14	650	11:25	48532.3	49065.5	533.2		Soil cover
15	700	11:26	48745.3	49065.5	320.2		Soil cover
16	750	11:27	48919.3	49065.5	146.2		Soil cover
17	800	11:29	48653.3	49065.5	412.2		Soil cover
18	850	11:31	48724.2	49064	339.8		Soil cover
19	900	11:32	48964.5	49064	99.5		Soil cover
20	950	11:34	48623.5	49064	440.5		Soil cover
21	1000	11:35	48622.1	49064	441.9		Soil cover
22	1050	11:36	48619.6	49064	444.4		Soil cover

Table S2. (Continued).

23	1100	11:38	48588.8	49065	476.2		Soil cover
24	1150	11:41	48586.4	49065	478.6		Soil cover
25	1200	11:43	48633	49072.8	439.8		Soil cover
26	1250	11:45	48794.2	49072.8	278.6		Soil cover
27	1300	11:47	48768.3	49065.6	297.3		Soil cover
28	1350	11:49	48879	49065.6	186.6		Soil cover
29	1400	11:51	49554.5	49065.6	–488.9	1962	Granite
30	1450	11:53	48776	49062.7	286.7	466	Granite
31	1500	11:56	48825.8	49062.7	236.9		Soil cover
32	1550	11:57	48861.7	49063.4	201.7	105	Granite
33	1600	11:59	48747.5	49063.4	315.9		Soil cover
34	1650	12:01	48870	49063.4	193.4		Soil cover
35	1700	12:03	48997.3	49065.6	68.3	1622	Granite
36	1750	12:05	49012.9	49065.6	52.7	3946	Granite
37	1800	12:09	48772.8	49062.9	290.1		Soil cover
38	1850	12:11	48834.5	49062.9	228.4	2798	Granite
39	1900	12:13	49032.7	49054	21.3		Soil cover
40	1950	12:15	48658.9	49054	395.1	3040	Granite
41	2000	12:17	48962.1	49062.7	100.6		Soil cover

Table S3. Values for to the B1-B2 magnetic measurement line.

Point	Horizontal scale (m)	Time	TMI	Magnetic field base value	Magnetic field anomaly	Susceptibility	Rock unit
0	0	13:06	48186.5	49075	888.5		Soil cover
1	50	13:08	48302	49075	773		Soil cover
2	100	13:09	48437.4	49073.2	635.8		Soil cover
3	150	13:10	48264.7	49073.2	808.5		Soil cover
4	200	13:12	48326.6	49073.2	746.6		Soil cover
5	250	13:14	48345.7	49073.2	727.5		Soil cover
6	300	13:16	48293.1	49073.2	780.1		Soil cover
7	350	13:17	48274.2	49073.2	799		Soil cover
8	400	13:19	48319.3	49073.2	753.9		Soil cover
9	450	13:20	48362.6	49073.2	710.6		Soil cover
10	500	13:22	48404.8	49073.2	668.4		Soil cover
11	550	13:23	48468.6	49073.2	604.6		Soil cover
12	600	13:25	48549	49072.2	523.2	122	Basalt
13	650	13:26	48602.8	49072.4	469.6		Soil cover
14	700	13:27	48392.6	49072.4	679.8		Soil cover
15	750	13:28	48743	49072.4	329.4		Soil cover
16	800	13:30	48336.3	49073.9	737.6		Soil cover

Table S4. (Continued).

17	850	13:32	48398.3	49073.9	675.6		Soil cover
18	900	13:33	48434.5	49073.9	639.4		Soil cover
19	950	13:34	48463.9	49073.5	609.6		Soil cover
20	1000	13:35	48491.3	49073.5	582.2		Soil cover
21	1050	13:38	48534.6	49073.9	539.3		Soil cover
22	1100	13:40	48616.2	49073.9	457.7		Soil cover
23	1150	13:42	48708.5	49073.9	365.4		Soil cover
24	1200	13:44	48442.3	49073.9	631.6		Soil cover
25	1250	13:45	48588.5	49073	484.5		Soil cover
26	1300	13:46	48714.4	49073	358.6		Soil cover
27	1350	13:48	48605.1	49073.4	468.3		Soil cover
28	1400	13:49	48704.8	49073.4	368.6		Soil cover
29	1450	13:53	48717.9	49073.4	355.5		Soil cover
30	1500	13:54	48786.5	49073.4	286.9		Soil cover
31	1550	13:55	48665.1	49064.8	399.7		Soil cover
32	1600	13:57	48703.4	49064.8	361.4		Soil cover
33	1650	13:59	48703.3	49063.6	360.3		Soil cover
34	1700	14:00	48787.7	49063.6	275.9		Soil cover
35	1750	14:02	48753.2	49063.6	310.4		Soil cover
36	1800	14:05	48716.8	49063.6	346.8		Soil cover
37	1850	14:06	49043.5	49063.6	20.1		Soil cover
38	1900	14:07	48964.4	49065	100.6		Soil cover
39	1950	14:08	48834.1	49065	230.9		Soil cover
40	2000	14:10	49035.6	49066.3	30.7		Soil cover
41	2050	14:11	49430.8	49066.3	–365		Soil cover
42	2100	14:13	48983.7	49066.3	82.6		Soil cover
43	2150	14:14	48819.1	49066.3	247.2		Soil cover
44	2200	14:16	48993.1	49064.4	71.3		Soil cover
45	2250	14:17	49188.5	49064.4	–124		Soil cover
46	2300	14:18	49262.4	49064.4	–198		Soil cover
47	2350	14:21	49448	49054	–394		Soil cover

Table S4. Values for to the C1-C2 magnetic measurement line.

Point	Horizontal scale (m)	Time	TMI	Magnetic field base value	Magnetic field anomaly	Susceptibility	Rock unit
1	0	17:17	48247.3	49085.1	837.8		Soil cover
2	50	17:18	48261.2	49085.1	823.9		Soil cover
3	100	17:20	48289.7	49085.1	795.4		Soil cover
4	150	17:24	48295.5	49083.6	788.1		Soil cover
5	200	17:26	48289	49083.6	794.6		Soil cover
6	250	17:28	48217	49087.3	870.3		Soil cover
7	300	17:33	48146.7	49083.7	937		Soil cover
8	350	17:35	48195.2	49083.7	888.5		Soil cover
9	400	17:37	48385.5	49088.7	703.2		Soil cover
10	450	17:40	48185.5	49088.7	903.2		Soil cover
11	500	17:42	48225.2	49086.8	861.6		Soil cover
12	550	17:43	48175	49086.8	911.8		Soil cover
13	600	17:45	48321.5	49086.8	765.3		Soil cover
14	650	17:46	48615.9	49086.8	470.9		Soil cover
15	700	17:47	48177.7	49088.1	910.4		Soil cover
16	750	17:50	48200.6	49088.1	887.5		Soil cover
17	800	17:52	48206.2	49087.7	881.5		Soil cover
18	850	17:53	48252.5	49087.7	835.2		Soil cover
19	900	17:54	48273.1	49087.7	814.6		Soil cover
20	950	17:56	48301.9	49087.7	785.8		Soil cover
21	1000	18:00	48336.7	49087.4	750.7		Soil cover
22	1050	18:01	48353.7	49087.4	733.7		Soil cover
23	1075	18:03	48350	49087.6	737.6		Soil cover
24	1100	18:06	48342.2	49087.6	745.4		Soil cover
25	1125	18:07	48336	49087.5	751.5		Soil cover
26	1150	18:08	48327.9	49087.5	759.6		Soil cover
27	1175	18:09	48313.4	49087.5	774.1		Soil cover
28	1200	18:10	48299.7	49087.5	787.8		Soil cover
29	1225	18:11	48309	49087.5	778.5		Soil cover
30	1250	18:12	48472.7	49087.5	614.8		Soil cover
31	1275	18:15	48511.8	49087.5	575.7		Soil cover
32	1300	18:17	48130	49088.3	958.3		Soil cover
33	1325	18:18	47983.9	49088.3	1104		Soil cover
34	1350	18:19	47138.3	49088.3	1950		Soil cover
35	1375	18:23	48256.6	49087.8	831.2		Soil cover
36	1400	18:24	48308.1	49087.8	779.7		Soil cover
37	1425	18:26	48283	49087.8	804.8		Soil cover
38	1450	18:29	48345	49087.6	742.6		Soil cover
39	1475	18:30	48327.9	49087.6	759.7		Soil cover
40	1500	18:31	48021	49087.6	1067		Soil cover
41	1525	18.3	48000	49088.1	1088		Soil cover

Table S4. (Continued).

42	1550	18:34	48200	49088.1	888.1		Soil cover
43	1575	18:35	48394.4	49088.1	693.7		Soil cover
44	1600	18:37	48407.6	49083.4	675.8		Soil cover
45	1625	18:38	48429	49083.4	654.4		Soil cover
46	1650	18:39	48455.4	49083.4	628		Soil cover
47	1675	18:41	48460	49083.4	623.4		Soil cover
48	1700	18:42	48452.4	49083.4	631		Soil cover
49	1725	18:43	48460.2	49084	623.8		Soil cover
50	1750	18:45	48523.8	49084	560.2		Soil cover
51	1775	18:46	48598.7	49084	485.3		Soil cover
52	1800	18:47	48705.5	49083.6	378.1		Soil cover
53	1825	18:50	48713.9	49083.6	369.7		Soil cover
54	1850	18:50	48552	49083.6	531.6		Soil cover
55	1875	18:51	48566	49083.6	517.6		Soil cover
56	1900	18:53	48720	49084.8	364.8		Soil cover
57	1925	18:54	48860.9	49084.8	223.9		Soil cover
58	1950	18:55	48963.1	49084.8	121.7		Soil cover
59	1975	19:04	48800.7	49082.5	281.8		Soil cover
60	2000	19:05	48617.5	49082.5	465		Soil cover
61	2025	19:06	48977.1	49082.5	105.4		Soil cover
62	2050	19:07	48616.5	49085.1	468.6		Soil cover
63	2075	19:08	48468.8	49085.1	616.3		Soil cover
64	2100	19:09	48506.4	49085.1	578.7		Soil cover
65	2150	19:10	48458.4	49085.1	626.7		Soil cover
66	2200	19:12	48341.5	49081.9	740.4		Soil cover
67	2250	19:13	48615.7	49081.9	466.2		Soil cover
68	2300	19:14	48742.2	49081.9	339.7		Soil cover
69	2350	19:15	48818.8	49081.9	263.1		Soil cover
70	2400	19:16	49026	49081.9	55.9		Soil cover
71	2450	19:18	48904.8	49082.4	177.6		Soil cover
72	2500	19:20	48947	49082.4	135.4		Soil cover
73	2550	19:21	49180.1	49082.4	–97.7		Soil cover
74	2600	19:23	49059.3	49082.4	23.1		Soil cover

Table S5. Values for to the D1-D2 magnetic measurement line.

Point	Horizontal scale (m)	Time	TMI	Magnetic field base value	Magnetic field anomaly	Susceptibility	Rock unit
1	0	8:20	48200	49076.4	876.4	3750	Basalt
2	25	8:25	48253.3	49075.7	822.4	108	Basalt
3	50	8:33	48257.3	49077.4	820.1		
4	75	8:34	48238.3	49077.4	839.1		
5	100	8:35	48198.6	49077.4	878.8		
6	125	8:37	48220.7	49076	855.3	1540	Basalt
7	150	8:39	48289.7	49076.4	786.7		
8	175	8:40	48233.3	49073.6	840.3		
9	200	8:42	48233.8	49073.5	839.7		
10	225	8:44	48218	49072.8	854.8		
11	250	8:45	48193.2	49072.8	879.6		
12	275	8:46	48166.7	49074.8	908.1		
13	300	8:46	48222.8	49074.8	852		
14	325	8:47	48342.9	49074.8	731.9		
15	350	8:48	48113.1	49073.7	960.6		
16	375	8:49	48254.6	49073.7	819.1		
17	400	8:50	48134.1	49073	938.9		
18	425	8:56	48081.7	49072.4	990.7	34	Limestone
19	450	9:03	48171.8	49072.2	900.4		
20	475	9:03	48197.6	49072.2	874.6		
21	500	9:07	48198.4	49073.2	874.8		
22	525	9:08	48177.7	49071.6	893.9		
23	550	9:09	48176.7	49071.6	894.9		
24	575	9:10	48186	49073.2	887.2	2	Limestone
25	600	9:11	48196.2	49073.2	877		
26	625	9:12	48191	49064.8	873.8		
27	650	9:15	48193.6	49073.3	879.7		
28	675	9:17	48200	49073.2	873.2		
29	700	9:18	48210.2	49072.3	862.1		
30	725	9:19	48215.8	49072.3	856.5		
31	750	9:20	48221.8	49066.2	844.4		
32	775	9:23	48221.1	49065.8	844.7		
33	800	9:25	48121.4	49066.4	945		
34	825	9:27	48215.8	49065.4	849.6		
35	850	9:28	48187.6	49067.2	879.6		
36	875	9:32	48153.5	49065.1	911.6		
37	900	9:33	48203.4	49065.1	861.7		
38	925	9:34	48236	49066.7	830.7		
39	950	9:35	48211.8	49066.7	854.9		
40	975	9:36	48347	49072.8	725.8	219	Granite
41	1000	9:41	48193.1	49071.6	878.5	693	Granite

Table S5. (Continued).

42	1025	9:43	48258.4	49071.8	813.4		
43	1050	9:44	48257.9	49071.3	813.4		
44	1075	9:45	48226	49071.3	845.3		
45	1100	9:47	48166	49071	905		
46	1125	9:49	48156.6	49072.7	916.1		
47	1150	9:51	48183.6	49070.6	887		
48	1175	9:52	48233.5	49073.1	839.6		
49	1200	9:53	48303	49073.1	770.1		
50	1225	9:54	48204.5	49070.5	866		
51	1250	9:56	48198	49072	874	78	Basalt
52	1275	9:57	48232	49072	840		
53	1300	9:58	48254.2	49071.6	817.4		
54	1325	9:59	48160	49071.6	911.6		
55	1350	10:01	48166.1	49072	905.9		
56	1375	10:02	48161.8	49071.9	910.1		
57	1400	10:03	48098.6	49071.9	973.3		
58	1425	10:04	48128.9	49071.5	942.6		
59	1450	10:05	48116.6	49071.5	954.9		
60	1475	10:06	48161	49071.1	910.1	745	Granite
61	1500	10:08	48329.9	49072.8	742.9		
62	1525	10:09	48066	49072.8	1007		
63	1550	10:10	48099	49071.9	972.9		
64	1575	10:13	48093.6	49072.1	978.5	694	Granite
65	1600	10.2	48120.8	49071.8	951		
66	1625	10:17	48115.4	49071.3	955.9		
67	1650	10:18	48247.4	49073	825.6		
68	1675	10:19	48173	49073	900		
69	1700	10:20	48133	49071.9	938.9		
70	1725	10:22	48153.3	49071.5	918.2		
71	1750	10:23	48137	49071.5	934.5		
72	1775	10:25	48136.1	49072.1	936		
73	1800	10:26	48148.1	49071.1	923		
74	1825	10.4	48151.6	49071	919.4		
75	1850	10:36	48137.7	49072.5	934.8		
76	1875	10:38	48191.3	49071.9	880.6	6	Limestone
77	1900	10:40	48195.2	49069.6	874.4		
78	1925	10:42	48205.5	49067.8	862.3		
79	1950	10:43	48219.1	49067.8	848.7		
80	1975	10:44	48228.8	49069.9	841.1		
81	2000	10:45	48128.5	49069.9	941.4		
82	2025	10:46	48239.9	49069.4	829.5		
83	2050	10:47	48048	49069.4	1021	1	Limestone
84	2075	10:50	48265.9	49074.7	808.8	1	Limestone

Table S5. (Continued).

85	2100	10:52	48283.8	49069.6	785.8		
86	2125	10:53	48284.9	49069.6	784.7		
87	2150	10:54	48353.7	49069	715.3		
88	2175	10.6	48367.5	49069	701.5		
89	2200	10:56	48455.5	49068.6	613.1		
90	2225	10:57	48518	49068.6	550.6		
91	2250	10:58	48621.6	49069.6	448		
92	2275	10:59	48698	49069.6	371.6		
93	2300	10:59	48529	49069.6	540.6		
94	2325	11:00	48520	49073.2	553.2		
95	2350	11:02	48506	49073.4	567.4		
96	2375	11:03	48483	49073.4	590.4		
97	2400	11:05	48406.7	49073.2	666.5		Limestone
98	2425	11:08	48424.8	49073.9	649.1		
99	2450	11:10	49133	49072.3	–60.7		Limestone
100	2475	11:12	48491	49073.5	582.5		
101	2500	11:12	48367	49073.5	706.5		
102	2525	11:13	48330.3	49073.5	743.2		
103	2550	11:14	48240	49072.9	832.9		
104	2575	11:15	48258	49072.9	814.9		
105	2600	11:15	48225	49072.9	848.3		
106	2625	11:16	48312	49073.3	761.5		
107	2650	11:17	48436	49073.3	637.8		
108	2675	11:18	48347	49073.1	726.3		
109	2700	11:19	48643	49073.1	429.8		
110	2725	11:35	48652	49066.9	415.1		
111	2750	11:36	48479	49066.9	587.9		
112	2775	11:37	49025	49066.9	41.9		
113	2800	11:38	49012	49068.9	56.9		
114	2825	11:39	48310	49068.9	758.9		
115	2850	11:40	48237	49068.5	831.5		
116	2875	11:41	47328	49068.5	1741		
117	2900	11:42	49706	49069.1	–637		
118	2925	11:44	48861	49067.9	206.7		
119	2950	11:45	50605	49067.9	–1537		
120	2975	11:46	49150	49068.4	-81.6		
121	3000	11:47	48652	49068.4	416.4		
122	3025	11:48	48340	49068	728		
123	3050	11:50	48354	49068.3	714.3		
124	3075	11:51	48170	49068.3	898.3		
125	3100	11:52	48431	49069.4	638.4		
126	3125	11:53	48293	49069.4	776.4		
127	3150	11:55	48410	49068.2	658.2		Limestone

Table S5. (Continued).

128	3175	11:56	48493	49069.7	577		
129	3200	11:57	48616	49069.7	453.6		Limestone
130	3225	11:58	48488	49068.5	580.3		
131	3250	11:59	49096	49068.5	–27.7		
132	3275	12:00	48972	49069.2	97.3		
133	3300	12:01	48807	49069.2	262.7		
134	3325	12:02	48615	49069.7	454.7		
135	3350	12:03	48574	49069.7	495.7		
136	3375	12:06	48457	49069.8	612.8		
137	3400	12:07	48421	49069.8	648.8		
138	3425	12:08	48441	49068.9	627.9		
139	3450	12:09	48383	49068.9	685.9		
140	3475	12:10	48379	49069	689.9		
141	3500	12:13	48357	49069	711.8		
142	3525	12:14	48312	49068.7	756.5		
143	3550	12:15	48341	49068.7	727.5		
144	3575	12:16	48350	49069.5	719.6		
145	3600	12:17	48339	49069.5	730.1		
146	3625	12:18	48349	49065.2	716.3		
147	3650	12:19	48373	49065.2	692.3		
148	3675	12.2	48376	49070.6	694.5		
149	3700	12:45	48399	46082.6	–2316		
150	3725	12:46	48413	49072.7	659.7		
151	3750	12:47	48449	49072.7	624.1		
152	3775	12:49	48453	49082	628.6		Basalt
153	3800	12:50	48478	49080.4	602.1		
154	3825	12:51	48526	49080.4	554.4		
155	3850	12:51	48600	49080.4	480.4		
156	3875	12:52	48694	49082.6	389		
157	3900	12:52	48828	49082.6	254.2		
158	3925	12:53	48922	49082.6	160.8		
159	3950	12:53	48992	49082.6	90.4		
160	3975	12:54	48998	49081.2	83.1		
161	4000	12:54	48938	49081.2	143.1		
162	4025	12:55	48912	49081.2	169.6		
163	4050	12:56	48797	49080.8	284		
164	4075	12:57	48900	49080.8	180.8		
165	4100	12:58	49400	49082.5	–318		
166	4125	13:00	49416	49073.5	–343		
167	4150	13:01	49970	49073.5	–896		
168	4175	13:02	48209	49073.4	864.5		
169	4200	13:03	47729	49073.4	1344		
170	4225	13:04	48012	49074.9	1063		

Table S5. (Continued).

171	4250	13:05	48152	49074.9	923.3		
172	4275	13:06	48339	49073.1	734		
173	4300	13:07	48430	49073.1	643.6		
174	4325	13:08	48430	49073.4	643.9		
175	4350	13:08	48407	49073.4	666.3		
176	4375	13:09	48283	49073.4	790.1		
177	4400	13:10	48518	49073.7	556		
178	4425	13:10	48383	49073.7	690.3		
179	4450	13:11	48423	49073.7	651.1		
180	4475	13:12	48729	49073	344.4		
181	4500	13:13	48831	49073	242.2		
182	4525	13:14	48784	49067.8	283.4		
183	4550	13:15	48788	49067.8	280.2		
184	4575	13:16	48634	49073.5	439.3		
185	4600	13:17	48747	49073.5	326.4		
186	4625	13:17	49047	49073.5	26.5		
187	4650	13:18	48711	49073.5	362.5		
188	4675	13:19	48691	49073.5	382.5		
189	4700	13:20	48741	49068.2	326.8		
190	4725	13:21	48542	49068.2	526		
191	4750	13:21	48576	49068.2	492.3		
192	4775	13:22	48615	49068.8	453.6		
193	4800	13:23	48641	49068.8	428.3		Limestone
194	4825	13:23	48674	49068.8	394.6		
195	4850	13:24	48755	49069.7	314.3		
196	4875	13:25	48762	49069.7	307.7		
197	4900	13:26	48740	49069.7	329.4		Limestone
198	4925	13:27	48740	49069.7	329.4		
199	4950	13:28	48712	49076.6	364.6		
200	4975	13:29	48724	49076.6	352.6		
201	5000	13:30	48766	49068.5	303		
202	5025	13:31	48861	49068.5	207.5		
203	5050	13:31	48806	49068.5	263		
204	5075	13:32	48760	49068.8	309.3		
205	5100	13:32	48678	49068.8	390.8		
206	5125	13:33	48774	49068.8	294.8		